41st Aerospace Sciences Meeting and Exhibit
6-9 January 2003, Reno, Nevada

AIAA 2003-1247

Design Optimization for Submerged Inlets- Part I

Ezgi S. Taskinoglu*, Doyle D. Knight†
Dept of Mechanical and Aerospace Engineering
Rutgers - The State University of New Jersey
98 Brett Road, Piscataway, NJ 08854-8058

This paper summarizes the computational analysis performed on a generic subsonic submerged inlet for the ultimate purpose of optimizing its design. A trade study consisting of four geometry deformations is investigated to obtain a meaningful initial geometry deformation for design optimization. The results are compared in terms of distortion indices which is an indication of the flow axisymmetry at the compressor face. In addition, a grid sensitivity analysis is performed to determine the effects of truncation errors involved in the numerical analysis. Future work will include an automated design optimization of a subsonic submerged inlet.

Introduction

The inlet of an air vehicle is an important component which affects not only the propulsion but also the aerodynamic characteristics of the vehicle. The inlet delivers the freestream air to the engine. In each phase of the flight envelope corresponding to different flow conditions ranging from subsonic to supersonic speeds, the inlet must provide an appropriate amount of the airflow to the engine. It retards the incoming flow and converts its kinetic energy into pressure. Although it does no work on the flow itself, it is responsible for the quality of the air at the face of the compressor which requires high total pressure energy and minimum distortion. In addition, since the inlet is included in the wetted area of the air vehicle, its shape and location directly affect the aerodynamic forces on the vehicle.

Hence, numerous research studies on the inlet shape and location has been conducted and various inlet types have been created.[1,2] The necessity of reducing the overall weight of air vehicle leads to short ducting bends and highly curved hump inlets. Examples of these kind of inlets are serpentine inlets, S-duct diffusers and submerged inlets. In all of these designs, the shape of the inlet, since it has an off center curvature or variation in cross-sectional area or out-of-plane bends, yields cross stream pressure gradients, which in turn produces secondary flows along the walls leading to flow separation and non uniform velocity gradients.

Rowe[3] made a detailed measurements on total pressure and yaw relative to the pipe axis in pipe bends for a velocity profile which is initially axisymmetric. However, at an air vehicle inlet entrance there is always a thin boundary layer. Thus, experimental research in the presence of thin inlet boundary layer had been conducted.[4] The resulting effect of inlet curvature on the compressor face is a nonuniform distribution of total pressure which is an indication of flow distortion. The reason of this distortion is explained by expulsion of the low energy fluid by a pair of contra-rotating vortices in the boundary layer and mixing of this low energy flow with the core flow.[4] Centerline curvature was found to be the main reason for distortion and losses in the S-ducts, while cross sectional area change had a negligible effect on flow quality and pressure loss.[5] An extensive experimental study for a representative S-duct configuration for the measurements of three dimensional velocity field and total and static pressures was performed for the purpose of supplying a comprehensive benchmark data set.[6] This study gave consistent results with the findings of the previous numerical and experimental studies and was used for validation of computational methods.

The research study done on serpentine inlets showed a similar result: duct curvature in the primary flow direction has the largest impact on inlet performance, while the duct cross-section shaping has a smaller impact.[7]

One of the methods to supress separation and therefore decrease total pressure variation across the exit face is to locate vortex generators near the entrance of the diffuser.[5,8,9] In this method vortices in the opposite direction to the secondary flow are generated to counteract the effect of secondary flow vortices.

Utilizing boundary layer control is another way to minimize the flow separation in inlets. Boundary layer suction, blowing and their combination are showed to lower the flow distortion by minimizing the separation in the inlet duct.[10]

An alternative method of minimizing exit distortion is to employ a shape optimization.[11,12] For S-duct diffusers a Gausian bump located before the separation region showed an improvement for flow distortion at the exit plane.[11] This study was pursued by an automated design optimization in which a design loop

*Graduate Student, Dept of Mechanical and Aerospace Engineering, Member, AIAA.

†Professor, Dept of Mechanical and Aerospace Engineering; Associate Fellow, AIAA.

was constructed by linking a flow solver with an optimizer to optimize S-shaped subsonic diffuser.[11,12] Zhang[11] explained the performance improvement seen in the diffuser by the suppression of detrimental secondary flows as a result of surface modification which redirected the flow. Lefantzi[12] emphasized the complex three dimensional flow separation in the bump by means of flowfield visualizations.

Automated shape optimization, i.e., coupling a CFD software with an optimization algorithm to determine better design shapes under several constraints, became a powerful design tool with the advent of powerful computers and advanced tehnologies. A two dimensional single-objective algorithm was employed to maximize the total pressure recovery of the missile inlet for a single flight point and mission. It is concluded in this study that in a short period of time it is possible to achieve improved inlet designs through the use of automated design optimization.[13] Repeating the same design optimization loop for the entire mission indicated that this powerful and innovative search process is capable of finding better inlet designs for specific missions with higher efficiency than conventional methods.[14] A similar design methodology for three dimensional supersonic inlet flow has been performed and placed into an industrial context.[15,16]

Although current research studies on serpentine inlets and S-duct diffusers can be found in the open literature, there are few studies performed directly on submerged inlets. The characteristic difference of submerged inlets is their placement flush to the fuselage, which yields lower drag and weight compared to the conventional inlets. Moreover, they have received considerable attention for military air vehicle applications because of their smaller radar cross sections and therefore ability to increase the survivability of the air vehicle.

Many research activities has been held on submerged inlets starting from early 1940s[17,18]. The behaviour of the flow in submerged inlets at various conditions including transonic speeds[19,20] and low supersonic speeds[21] was investigated. The effect of design variables, namely drag and pressure recovery[22] was studied. Various wind-tunnel tests were made on scaled fuselage models of a typical fighter aircraft.[23–25] In addition, large scale characteristics of a submerged inlet was examined for an inlet installed on a test fighter in the Ames 40-by 80-foot wind tunnel.[26–28] An extensive archive of the studies for which a limited number of references given above can be found in National Advisory committee for Aeronautics (NACA) digital library.[29] A numerical analysis has shown that this type of inlet similar to S-duct diffusers and serpentine inlets experiences nonuniform exit flow due to separation.[30]

For design optimization of this kind of inlets a necessary first step is to perform a trade study. For this purpose we have investigated different geometrical shape deformations of a generic submerged inlet. This paper summarizes the trade study performed for subsonic submerged inlet design optimization. The objective of the optimization is to achieve minimum flow distortion at the compressor face. A subsequent proposed paper[31] will describe the design optimization process and results.

1. NUMERICAL APPROACH

Description of the Inlet Geometry

In this study, the baseline geometry is chosen to be the generic submerged inlet shown in Fig. 1. Top view, side view, and back view of the generic inlet are given Figures 1(a), 1(b), 1(c), respectively. The representative air vehicle is a long ogive cylinder (Fig. 2) on which submerged inlet is mounted (Fig. 3). Numerical computations are performed by splitting the whole flow domain into two sections (Fig. 4). The forebody section is the axisymmetric body upstream of the inlet opening and it has an overlapped region with the channel section. Solid modelling for the submerged inlet geometry is done by the computer aided design program Pro/Engineer, Release 20.[32]

Mesh Generation

Grid generation of the flow domain is performed by the commercial software GRIDPRO/az3000.[33] This general purpose elliptic mesh generator creates three dimensional, multi-block structured grid by a variationally-based method with an iterative updating scheme. The user input for GRIDPRO are the surface geometry and the block topology. After the grid for the inviscid flow analysis is obtained, clustering near the wall region can be done by specifying the first cell height and the stretching ratio.

The generated grid for the channel section typically consists of eight blocks (Fig. 5) and approximately 260,000 nodes.

Flow Solver

The flow solver used is GASPex, Version 4.1.0+,[34] which solves the Reynolds-averaged compressible time dependent Navier Stokes equations in three dimensions. It utilizes a finite volume spatial discretization in which the state variables are stored at the cell centers. The accuracy of reconstructing the primitive variable field at the cell faces determines the spatial accuracy of the solution. The MUSCL approach is performed for variable extrapolation.

In our computations, the inviscid flux scheme is Roe's Method with third-order spatial accuracy reconstruction using the Min Mod limiter. Turbulence is modeled by the Wilcox $k-\omega$ model. A steady state solution is obtained by applying Gauss-Seidel relaxation scheme.

Boundary and Initial Conditions

The freestream conditions are shown in Table 1. They are chosen to correspond to the experimental conditions in the Rutgers Low Speed Wind Tunnel since a subsequent experimental study will be performed for comparison with the simulations. Although the Mach number is considerably less than typical flight Mach numbers for subsonic air vehicles with submerged inlets, the purpose of this study is to demonstrate the *methodology* of combined experimental and computational design optimization of submerged subsonic inlet. Inflow boundary conditions are prepared from the numerical solutions of the axisymmetric forebody upstream of the inlet. As an outflow boundary condition, back pressure equal to the freestream static pressure of 99kPa is specified at the exit of the diffuser. The computations are started impulsively from freestream conditions given in Table 1.

Table 1 Flow Conditions

Pressure p_∞ (kPa)	99
Density ρ_∞ (kg/m^3)	1.20
Temperature T_∞ (K)	288
Mach number M_∞	0.15

Figure of Merit

In this study, the figure of merit is chosen to be the flow distortion at the exit of the diffuser and it is calculated over the diffuser cross section (Fig. 6) as follows:

$$DC(\phi,\psi) = \max \frac{\bar{p}_0 - \bar{p}_0(\phi,\psi)}{\bar{q}}, 0 < \phi \leq 2\pi \qquad (1)$$

where p_0 is the total pressure, q is the dynamic pressure, and ϕ is the starting angle for a pie segment of angle ψ of the diffuser exit. It is:

$$\bar{p}_0 = \frac{\int_0^{2\pi}\int_0^R p_0(r,\theta) r dr d\theta}{\int_A dA}$$

$$\bar{p}_0(\phi,\psi) = \frac{\int_0^{\psi}\int_0^R p_0(r,\phi+\theta) r dr d\theta}{\int_\phi dA}$$

$$\bar{q} = \frac{\int_A q dA}{\int_A dA}$$

3. RESULTS and DISCUSSION

Baseline Submerged Inlet Results

Numerical simulations for the baseline submerged inlet have been performed with the freestream conditions given in Table 1. The exit back pressure of the diffuser is 99kPa which is equal to the freestream static pressure. On the basis of a 1-D inviscid analysis, this corresponds to a unit area mass flow rate of $q = 0.25$ which is defined as $q = \rho u/\rho^* u^*$ where ρ is the density, u is the velocity, and the supercript * represents the sonic conditions.

Computational results are presented in terms of surface streamlines (Fig. 7), streamwise velocity contour plots (Fig. 8) and total pressure contour plots (Fig. 9) with volume streamlines along the channel section.

The surface streamlines display lines of separation (L_S) on both sides of the symmetry axis tracing the flow separation.[35] As the flow moves down in the channel the adverse pressure gradient on the upper duct decelerates the flow and causes boundary layer separation. The boundary layer grows on the upper duct along the channel, whereas on the lower duct there already exists a thin boundary layer at the entrance of the channel section. The low momentum fluid on the lower duct escapes to the region with low static pressure on the upper duct and due to the separation it convects towards the center of the duct degrading the uniformity (Fig. 8). It is evident in Fig. 8 that the boundary layer on the lower duct gets thinner whereas that on the upper duct thickens along the channel expelling the low energy fluid into the core flow. This low velocity region corresponds to a low total pressure region in Fig. 9. In this figure at the exit cross section there is an upside down mushroom shape which is a typical flow pattern seen in curved bends. The mechanism that produces the low total pressure region, seen at the exit cross section as a mushroom shape, is a redistribution of vorticity in the incoming boundary layer due to secondary pressure gradients caused by the duct curvature (i.e., an inviscid rotational phenomenon).

It should be noted that the variation in total pressure at the exit cross section is within 1% only, whereas the variation in velocity is almost 50% indicating a high flow distortion.

Grid Sensitivity Analysis

The design optimization process of a submerged inlet requires the flow domain solution in every iteration of the design loop. It is important to decide the grid size sufficient to solve the flow domain accurately and small enough to save computational time. To be able to decide the sufficient number of grid points, a grid sensitivity analysis for our specific problem is necessary. The purpose of the study is to determine the effects of truncation errors involved in the numerical analysis of a generic submerged inlet (Fig. 1). For this purpose, the mesh sequencing option of commercial software package GASPex version 4.1.0+ is used. Five successive sequences are done and distortion indices at the exit cross section are calculated and compared. Table 2 gives the grid dimensions for coarse, medium, fine, finer and finest grid run definitions. The resulted values of distortion index in Table 2 displays

Table 2 Grid Points and Distortion Index

Grid	#Grid Points	Distortion Index
Coarse	18,176	0.3715
Medium	145,408	0.3760
Fine	466,944	0.3813
Finer	557,056	0.3817
Finest	1,163,264	0.3789

that the truncation error is negligibly small for baseline inlet. Therefore in our subsequent calculations a grid of 260,000 nodes which is in between medium and fine grid is used.

Trade Study

A trade study is an essential prerequisite for an automated design optimization. The purpose of the trade study is to gain physical insight into the effect of specific types of shape deformations on the optimization parameter (i.e., distortion index). The results of the trade study may be positive (i.e., shapes are found which reduce the distortion index) or negative (i.e., the opposite). Nevertheless, the results lead to both understanding and provide insight to the type of shape changes to be considered with automated design optimization.

Having obtained the solutions for the generic inlet, we deformed the surface by introducing bumps (Figures 10- 12) to several location of the baseline duct surface and a ring (Fig. 13) on the channel. For each newly deformed geometry, flow domain solutions are obtained in order to investigate the effect of the geometrical change on the distortion value. It should be noted that for each type of geometry deformation corresponding baseline geometry differs. This change is the result of the different techniques used for creation of the deformed geometry. Our calculations are tabulated in (Table 3).

Table 3 Distortion

Baseline Geometry	0.40
Upper Bump Deformation	0.39
Lower Bump Deformation	0.36
Baseline Geometry	0.35
Side Bump Deformation	0.31
Baseline Geometry	0.42
Ring Deformation	0.39

When a bump is located on the upper duct at the separation point found in baseline geometry flow domain computations, a reverse flow occurs in the bump (Fig. 14). Most of the singularities shown in surface streamline plot (Fig. 15) are due to placement of the bump. The line of separation is carried to the symmetry axis by this deformation. Examination of total pressure distribution at the exit cross section indicates the core energy is reduced and the low energy region is larger (Fig. 22). The velocity distribution, similarly, has a wider area of low velocity (Fig. 23).

The lower bump placement, on the other hand, brings the separation lines back to their place in baseline inlet. The direction of the lines of separation on both sides of the centerline is towards the symmetry axis (Fig. 17). Similar to the upper bump case, a vortex is generated in the bump (Fig. 16). The distortion is lower than the baseline distortion but this is due to the low total pressure and velocity value at the exit cross section (Figs. 22, 23). Although there is a decrease in distortion index value for lower bump configuration, it can be noticed by examination of volume streamlines that the flow behaviour did not change much. The reason for this is the decrease in total pressure level due to energy loss in the bump.

The side bump configuration given in Fig. 12 lowers the distortion index as well. The low energy region seen at the exit cross section is even wider, the low momentum fluid convected into the core flow further below the center (Figs. 22, 23). Lines of separations on both sides of the centerline shows a flow distortion that is parallel to the symmetry axis (Fig. 19). Fig. 18 displays a wide range of distorted flow.

By implementing a ring configuration given in Fig. 13 the flow which first enters the ring on the lower duct has been directed upwards and gathered with the low energy flow in the upper ring (Fig. 20). Similar to the other deformations, total pressure and velocity at the exit cross section is lower than baseline inlet (Figures 22, 23). Flow separation occurs on the symmetry axis (Fig. 21).

The secondary flows induced by pressure gradients due to curvature of the duct evolves into a pair of counter-rotating vortices along the duct. These vortices convects the low energy flow in the boundary layer into the high energy core flow. It is seen in Fig. 24 that the location of the vortices moved towards the center of the duct for deformed geometries.

4. CONCLUSIONS AND FUTURE WORK

This study has been done in order to investigate the effect of geometrical deformations on the flow behaviour. The main goal is to choose a deformation type which is promising to improve the distortion index value at the face of the compressor. Completion of this study will guide us to start the automated design optimization algorithm in which the baseline inlet geometry is going to be deformed in an automated way and its flow field is analyzed as it is deformed.

The trade study examined four different types of shape deformations (upper, lower, side and ring). The side deformation gave the largest percentage reduc-

tion in distortion (11%). Further trade studies are in progress and will be completed shortly.

The optimization will consist of two phases. The first phase is the single objective optimization problem at zero angle of attack and zero sideslip. The second phase is a multi objective design optimization problem in which the effect of varying angle of attack and sideslip on the inlet performance is going to be investigated.

In order to speed up the design process the cpu intensive part of the design loop (the flow domain solution) will be performed on the NCSA (The National Center for Supercomputing Applications) I32A Linux clusters. To integrate this component into the design loop it is necessary to implement so called "grid computing" tools. Grid computing is a technique basically for harnessing geographically distributed resources together.[36] In our study we will make use of Globus Toolkit for our Grid application. Globus Toolkit is the de facto standard for grid computing, it includes tools for authentication, scheduling, file transfer and resource description.[37]

Comparison of the numerical results with experimental data is necessary to verify the computational study. An experimental study for the same submerged inlet configuration has been started in collaboration with an experimental group in Rutgers University.

5. ACKNOWLEDMENT

This research is supported by the National Science Foundation under Grant No. NSF-CTS-0121058 monitored by Drs. Frederica Darema, C. F. Chen and Michael Plesniak. The authors would like to thank Prof. G. Elliott and Vasilije Jovanovic for supplying rapid prototyping models.

References

[1]J. Seddon, E. L. Goldsmith. Intake Aerodynamics. *AIAA Educational Series*, 1985.

[2]E. L. Goldsmith, J. Seddon. Practical Intake Aerodynamic Design. *AIAA Educational Series*, 1993.

[3]M. Rowe. Measurements and Computations in Pipe Bends. *Journal of Fluid Mechanics*, Vol 43, p 771, 1970.

[4]P. Bansod and P. Bradshaw. The Flow in S-Shaped Ducts. *Aeronautical Quarterly*, 23:131–140, 1972.

[5]L. A. Povinelli, and C. E. Towne. Viscous Analyses for Flow Through Subsonic and Supersonic Intakes *NASA TM 88831*, Sept. 1986.

[6]S. R Wellborn, B. A Reichert, and T. H. Okiishi. An Experimental Investigation of the Flow in a Diffusing S-duct. *AIAA-92-3622*, 1992.

[7]D. W. Mayer, B. H. Anderson, and T. A. Johnson. 3D Subsonic Diffuser Design and Analysis. *AIAA 98-3418*, July 1998.

[8]B. A. Reichert and B. J. Wendt. An Experimental Investigation of S-Duct Flow Control Using Arrays of Low-Profile Vortex Generators. *AIAA-93-0018*, 1993.

[9]B. A. Reichert and B. J. Wendt. Improving Curved Subsonic Diffuser Performance with Vortex Generators. *AIAA Journal*, 34(1):65–72, 1996.

[10]D .K Harper, T. A. Leitch, W. F. Ng, S. A. Guillot. Boundary Layer Control and Wall-Pressure Fluctuations in a Serpentine Inlet *AIAA Paper 2000-3597*, 2000.

[11]W. Zhang, D. Knight and D. Smith. Automated Design of a Three Dimensional Subsonic Diffuser. *Journal of Propulsion and Power*, Vol. 16, No. 6, 2000, pp. 1132-1140.

[12]S. Lefantzi, D. D. Knight. Automated Design Optimization of a Three-Dimensional S-Shaped Subsonic Diffuser. *Journal of Propulsion and Power*, Vol. 18, No. 4, 2002, pp. 913-921.

[13]M. Blaize, D. D. Knight. Automated Optimization of Two Dimensional High Speed Missile Inlets *AIAA Paper 1998-0950*, Jan. 1998.

[14]M. Blaize, D. D. Knight, K. Rasheed, X. Montazel, Y. Kergaravat. Optimization of Supersonic Missile Inlets Over Entire Mission. *82nd AGARD Fluid Dynamics Panel Symposium*, May 1998.

[15]C. Bourdeau, G. Carrier, D. Knight. Three Dimensional Optimization of Supersonic Inlets. *AIAA Paper 99-2108*, June 1999.

[16] G. Carrier, C. Bourdeau, D. Knight, Y. Kergaravat, X. Montazel. Multi-Flight Condition Optimization of Three-Dimensional Supersonic Inlets. *RTO AVT Symposium on Aerodynamic Optimization*, Ottawa, Canada, 1999.

[17]J. V. Becker,and D. D. Baals. Wind Tunnel Tests of A Submerged-Engine Fuselage Design. *NACA WR-L-485*, Oct., 1940.

[18]C. W. Frick, W. F. Davis, L. M. Randall, and E. A. Mossman. An Experimental Investigation of NACA Submerged-Duct Entrances. *NACA ACR-5120*, Nov., 1945.

[19]J. A. Axelson,and R. A. Taylor. Preliminary Investigation of the Transonic Characteristics of an NACA Submerged Inlet. *NACA RM-A50C13*, June, 1950.

[20]A. H. Sacks, and J. R. Spreiter. Theoretical Investigation of Submerged Inlets at Low Speed. *NACA TN-2323*, Aug., 1951, pp. 38,40,42.

[21]E. Anderson,and A. C. Frazer. Investigation of an NACA Submerged Inlet at Mach Numbers from 1.117 to 1.99. *NACA RM-A52F17*, Sept. , 1952.

[22]M. R. Nichols, and P. K. Pierpont. Preliminary Investigation of a Submerged Air Scoop Utilizing Boundary-Layer Suction to Obtain Increase Pressure Recovery. *NACA TN 3437*, Apr., 1955, pp. 76.

[23]N. K. Delany. An Investigation of Submerged Air Inlets on a 1/4-Scale Model of a Typical Fighter-Type Airplane. *NACA RM A8A20*, 1948, pp. 48.

[24]E. A. Mossman, and D. E. Gault. Development of NACA Submerged Inlets and Comparison with Wing Leading-Edge Inlets for 1/4-Scale Model of a Fighter Airplane. *NACA RM A7A31*, 1947, pp. 44.

[25]D. E. Gault. An Experimental Investigation of NACA Submerged Air Inlets on a 1/5-Scale Model of a Fighter Airplane. *NACA RM A7I06*, Dec. 05, 1947, pp. 35.

[26]N. J. Martin. Tests of Submerged Duct Installation on a Modified Fighter Airplane in the Ames 40- By 80-Foot Wind Tunnel. *NACA RM A8F21*, Dec. 11, 1947, pp. 25.

[27]N. J. Martin, and C. A. Holzhauser. An Experimental Investigation at Large Scale of Several Configurations of an NACA Submerged Air Intake. *NACA RM A8F21*, Oct. 19, 1948, pp. 69.

[28]C. A. Holzhauser. An Experimental Investigation at Large Scale of an NACA Submerged Intake and Deflector Installation on the Rearward Portion of a Fuselage. *NACA RM A50F13*, Aug. 30, 1950, pp. 24.

[29]NACA Digital Library, [Online] http://naca.larc.nasa.gov/

[30]E. Taskinoglu, D. Knight. Numerical Analysis of Submerged Inlets. *AIAA Paper 2002-3147*, June, 2002.

[31]E. Taskinoglu, D. Knight. Automated Design Optimization of a Subsonic Submerged Inlet. *Submitted to 21st Applied Aerodynamics Conference*, June, 2003.

[32]Parametric Technology Corporation. *Pro/Engineer User's Guide*, 1996.
[33]Program Development Corporation, White Plain, New York. *GridPro/az3000 User's Guide and Reference Manual*, 1998.
[34]Aerosoft Inc. *General Aerodynamic Simulation Program User Manual*, 1996.
[35]M. Tobak and D. J. Peake. Topology of Three-Dimensional Seperated Flows. *Ann. Rev. Fluid Mech.*, 1982. 14:61-85
[36] [Online] http://www.gridcomputing.com, 2002.
[37] [Online] http://www.globus.org

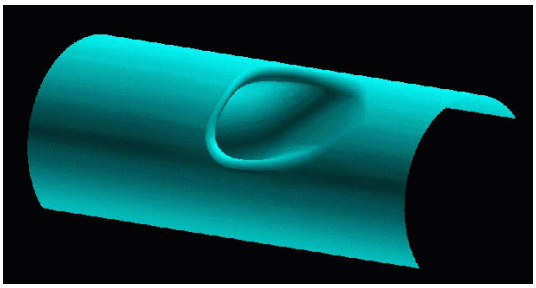

a) Top View

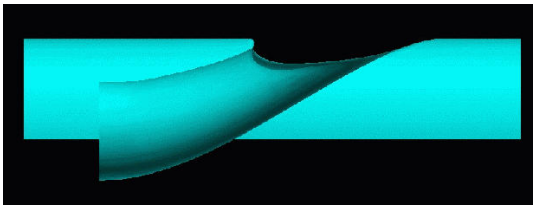

b) Side View

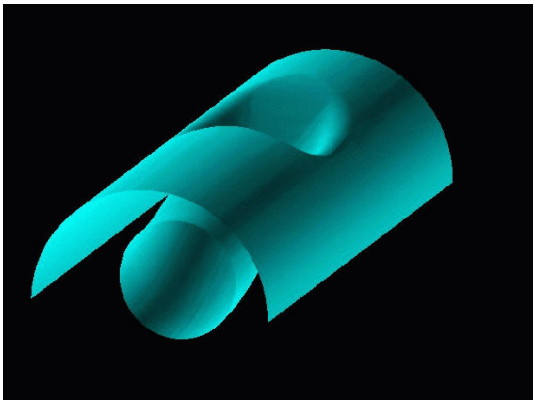

c) Back View

Fig. 1 Generic Inlet

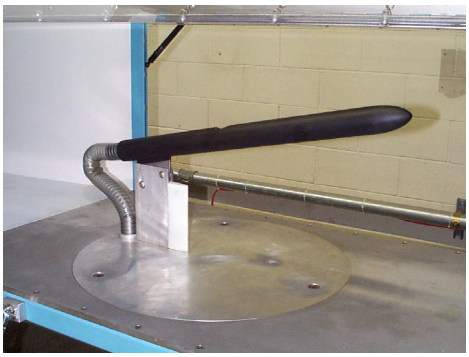

Fig. 2 Ogive Cylinder Model

Fig. 3 Model of Submerged Inlet

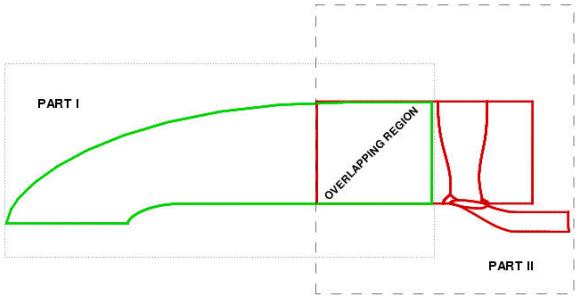

Fig. 4 Flow Domain

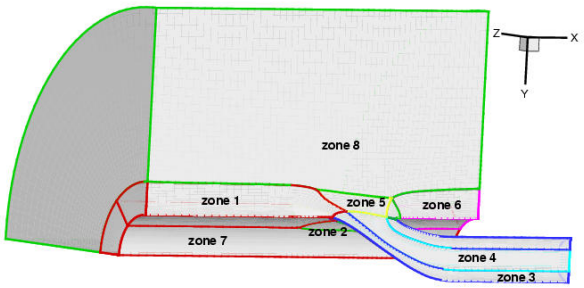

Fig. 5 Flow Domain for the Channel Section

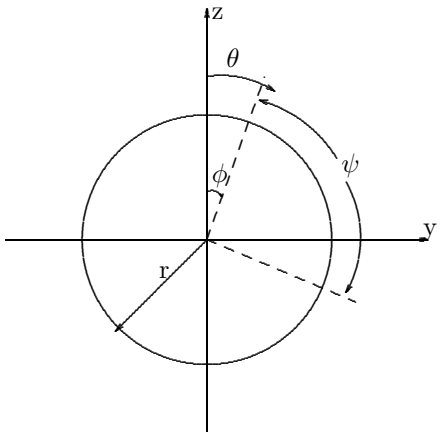

Fig. 6 2D Exit Cross Section of the Inlet

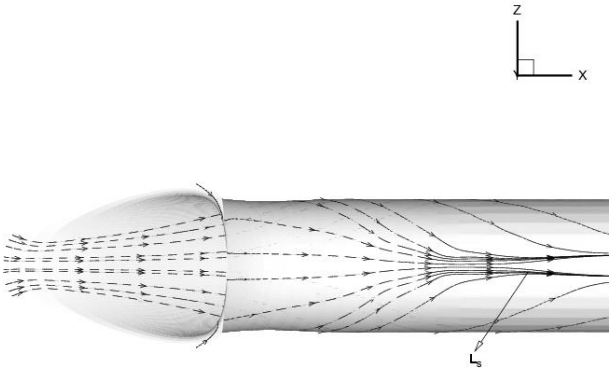

Fig. 7 Top View of Surface Streamlines for Baseline Inlet

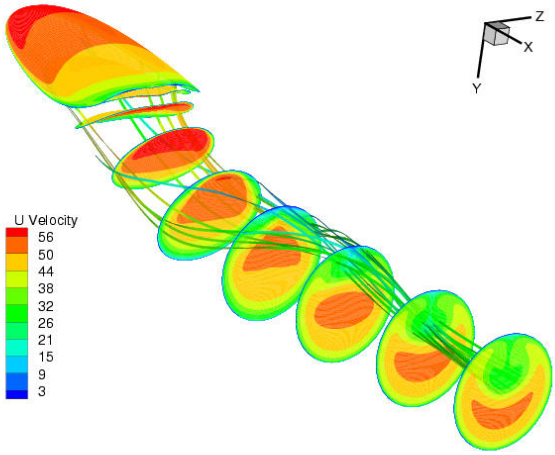

Fig. 8 Velocity Contour Plots with Streamlines in the Channel for Baseline Inlet

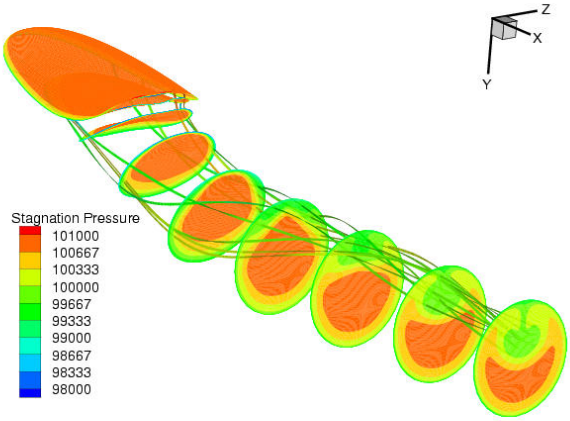

Fig. 9 Total Pressure Contour Plots with Streamlines in the Channel for Baseline Inlet

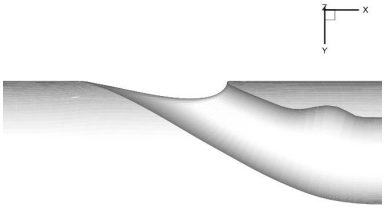

Fig. 10 Upper Bump Deformed Geometry

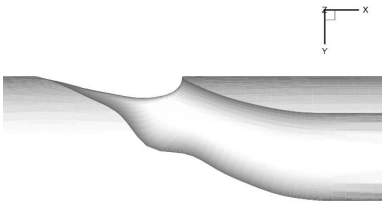

Fig. 11 Lower Bump Deformed Geometry

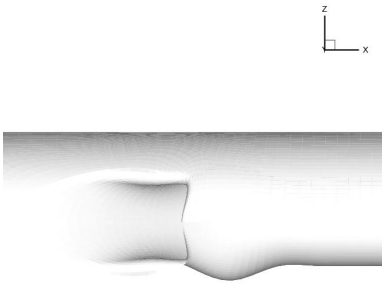

Fig. 12 Side Bump Deformed Geometry

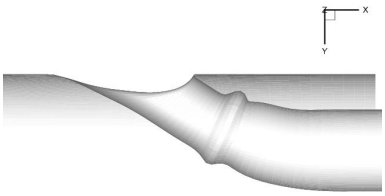

Fig. 13 Ring Deformation

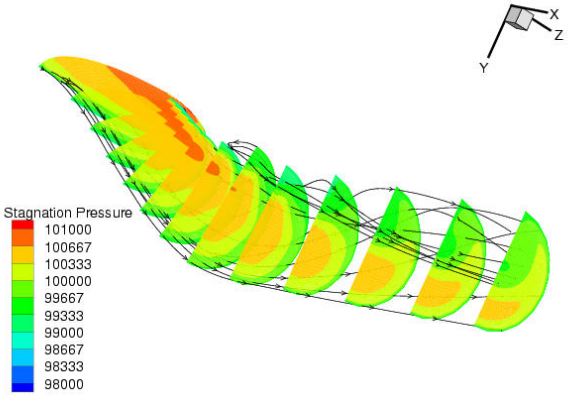

Fig. 14 Total Pressure Contour Plots with Streamlines in the Channel for Upper Bump Deformation

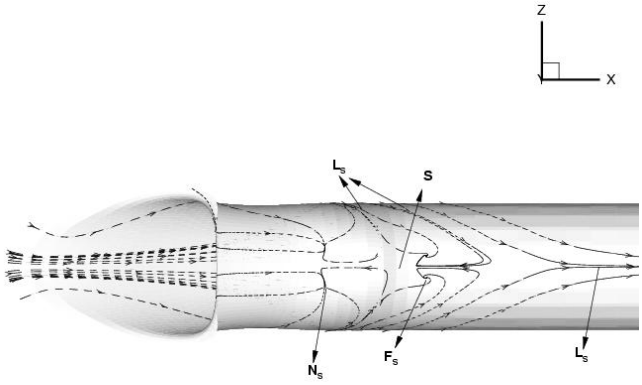

Fig. 15 Top View of Surface Streamlines for Upper Bump Deformation

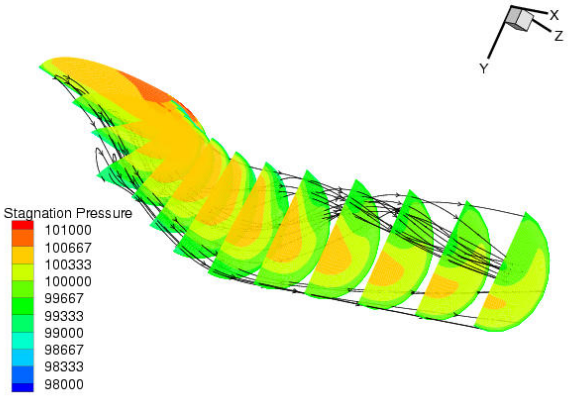

Fig. 16 Total Pressure Contour Plots with Streamlines in the Channel for Lower Bump Deformation

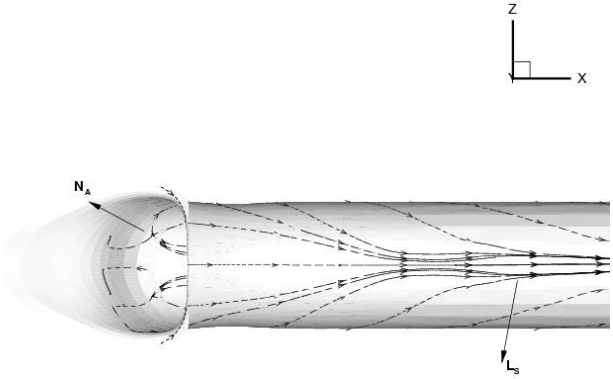

Fig. 17 Top View of Surface Streamlines for Lower Bump Deformation

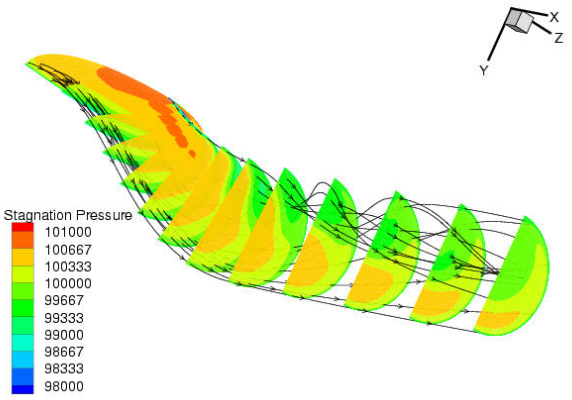

Fig. 18 Total Pressure Contour Plots with Streamlines in the Channel for Side Bump Deformation

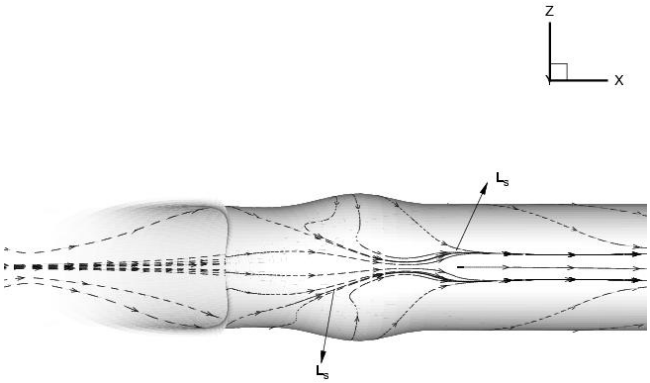

Fig. 19 Top View of Surface Streamlines for Lower Bump Deformation

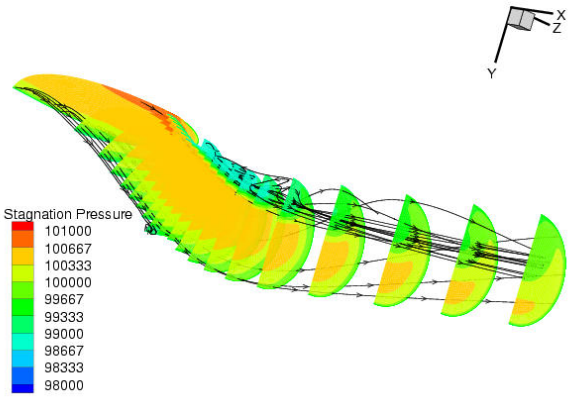

Fig. 20 Total Pressure Contour Plots with Streamlines in the Channel for Ring Deformation

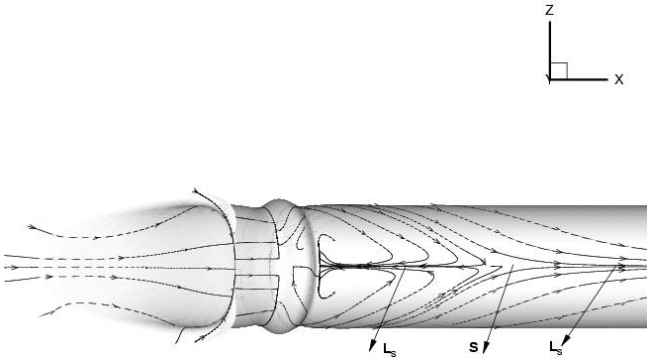

Fig. 21 Top View of Surface Streamlines for Ring Deformation

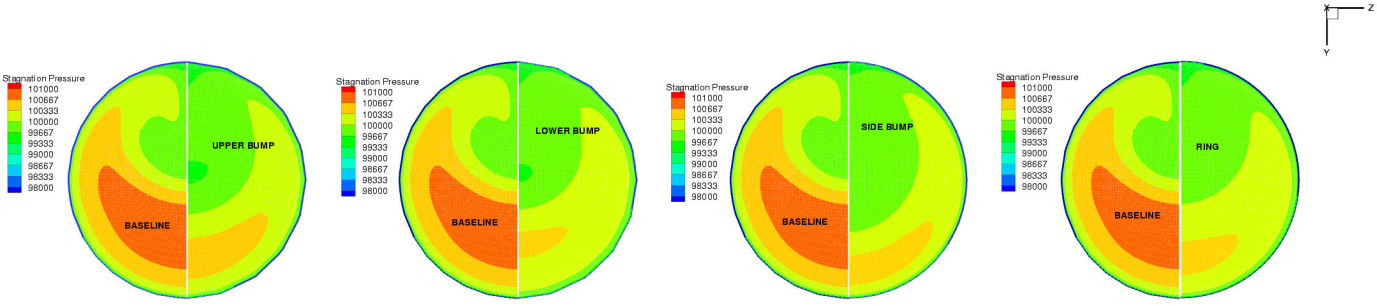

Fig. 22 Comparison of Total Pressure Distribution at the Exit Cross Section

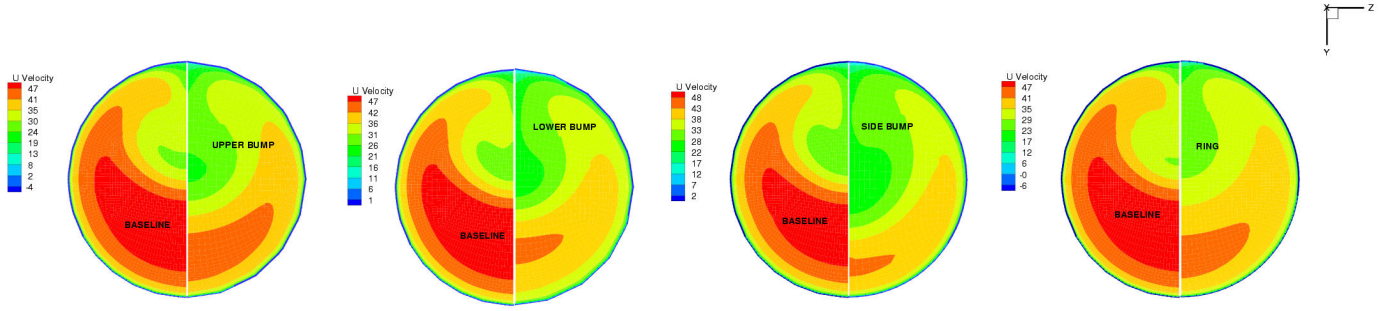

Fig. 23 Comparison of Velocity Distribution at the Exit Cross Section

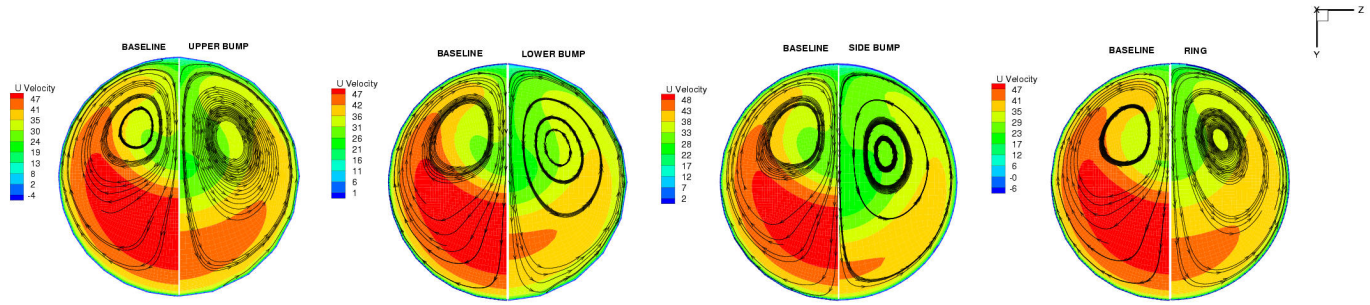

Fig. 24 Counter-rotating Vortices at the Exit Cross Section